R & M No. 3847

R & M No. 3847

PROCUREMENT EXECUTIVE, MINISTRY OF DEFENCE

Aeronautical Research Council
Reports and Memoranda

WIND-TUNNEL MEASUREMENT OF LATERAL AERODYNAMIC DERIVATIVES USING A NEW OSCILLATORY RIG, WITH RESULTS AND COMPARISONS FOR THE GNAT AIRCRAFT

by

C.O. O'Leary
Aerodynamics Department, RAE Bedford

London: Her Majesty's Stationery Office
£10 NET

UDC 533.6.013.42 : 533.6.071 : 533.6.082.3

WIND-TUNNEL MEASUREMENT OF LATERAL AERODYNAMIC DERIVATIVES USING A NEW OSCILLATORY RIG, WITH RESULTS AND COMPARISONS FOR THE GNAT AIRCRAFT

By C. O. O'Leary

Aerodynamics Department, RAE Bedford

REPORTS AND MEMORANDA No.3847*

October 1977

SUMMARY

The investigation of aircraft handling characteristics at high angle of attack and high subsonic speeds is hampered by the lack of accurate data on aerodynamic derivatives. The development of a rig and method of test for the measurement of oscillatory lateral aerodynamic derivatives under these conditions is described. Tests were made on a 0.16 scale model of a Gnat T Mk 1 aircraft and the results compared with those from wind-tunnel static tests, flight tests and estimates. Agreement with the other data is reasonably close except in the case of some cross damping derivatives. The accuracy of measurement of derivatives due to rate of roll should be improved by a proposed re-design of the excitation system.

* Replaces RAE Technical Report 77159 - ARC 37724

LIST OF CONTENTS

1 INTRODUCTION

In recent years there has been increased emphasis on the operation of combat aircraft near the limits of the flight envelope. In particular, there is a requirement for flight at high angles of attack at high subsonic Mach numbers. There is, therefore, a need to investigate handling characteristics in these conditions but such investigations are hampered by the lack of data on aerodynamic derivatives. A number of techniques for estimating derivatives are currently used but, in general, these techniques are inadequate at transonic Mach numbers and limiting angles of attack.

For a number of years the longitudinal and lateral aerodynamic derivatives of wind-tunnel models have been measured at RAE using an oscillatory rig. The models have been sting mounted on specially designed spring units and tests have been made over a range of Mach numbers between M = 0.1 and M = 2.8 in three different wind tunnels[1]. These tests have, however, been limited in the total normal force which could be applied to the sting (about 4.5 kN). Thus, it has been necessary to limit either angle of attack or Reynolds number, or both, to keep the normal force down. Under limiting flight conditions of combat aircraft it is considered that Reynolds number may have a significant effect on the derivatives. A spring unit capable of supporting a model at high subsonic Mach number and high total pressure was therefore designed, and manufactured. Tests of the unit were performed in the 8ft × 8ft wind tunnel using a 0.16 scale model of the Gnat aircraft. This model was chosen because the oscillatory test results could be compared with:

(a) results from flight tests made during an investigation of lateral stability of the Gnat aircraft at high angle of attack at high subsonic speeds,

(b) wind-tunnel static test results, and

(c) estimates of derivatives using methods available for conventional configurations such as the Gnat.

The Report first describes the established method of test, the design aims of the new spring unit and drive system, and the calibration technique used. Details of the wind-tunnel tests are then given and results compared with the other measurements and estimates. From this, it is concluded that the rig can be used to measure the small amplitude lateral derivatives of a wind-tunnel model with reservations only on the accuracy of the cross derivatives, sideforce and

yawing moment due to rate of roll. A modification to the rig to improve accuracy in this respect is described in a final section on future developments.

2 METHOD OF TESTING

The method of testing with the oscillatory rig is basically as described in Ref 1. Sufficient developments have taken place since that report was written, however, to warrant the inclusion here of a brief account of the current technique for lateral derivative measurement.

The model is mounted on a special sting or spring unit (Fig 1) which has a forward spring providing flexibilities in yaw and roll and a rear spring providing flexibility in sideslip. Oscillations are excited by means of an electromagnetic vibration generator and the motion is measured by means of strain gauges on the front and rear springs. The system has three modes of oscillation, A, B and C which are designated 'yawing', 'sideslipping' and 'rolling' modes respectively. The yawing mode is an oscillation mainly about a z-axis near the CG of the model whereas in the sideslipping mode the axis of oscillation is generally well forward of the nose of the model. The rolling mode is almost entirely an oscillation about the x-axis. It is possible to obtain a complete set of lateral derivatives from pure yaw and roll motions alone but flexibilities to allow all three modes of oscillation are deliberately designed into this rig. Complete elimination of the tendency for sideslipping motions to occur in a sting is difficult so the deliberate provision of a flexibility, which gives a predictable mode of oscillation at a desired frequency, is thought to be preferable.

The test procedure is to oscillate the model at or near the natural frequency of each mode in turn, since this is the only way of obtaining reasonable amplitudes with the small excitation force available. Eighteen derivatives are obtained by solving the complete equations of motion, using measured displacements, excitation inputs and frequencies, together with previously determined values of the model inertias. Current calibration procedures for determination of inertias and excitation constants are described in section 5 and Appendix A. The required aerodynamic derivatives are obtained as the differences between wind-off and wind-on values of the derivatives; assuming that the mechanical characteristics of the system are unaffected by the air loads. Since the frequencies are different for the different modes, it is necessary when solving the equations of motion to assume that the derivatives are independent of frequency. This procedure is not strictly correct since, in general, the derivatives always depend on frequency to some extent, but it is considered adequate because, in

effect, each derivative is obtained primarily from one of the modes with only small correction terms from the others. Also, the frequencies of the three modes are generally low enough, from an aerodynamic viewpoint, for the change in derivatives with frequency to be negligible.

3 DESIGN OF NEW SPRING UNIT

Although it was designed primarily for use in the 8ft × 8ft wind tunnel at RAE Bedford, the new spring unit can also be used in other tunnels of similar size. The total length of the sting, consisting of spring unit plus rear support section, was determined by the geometry of the 8ft × 8ft tunnel quadrant which rotates about a centre 1.9 m from its leading edge. The design requirements were as follows:

(1) The unit was required to have flexibilities which would allow three modes of oscillation, known as yaw, roll and sideslip.

(2) The amplitude of yaw and roll oscillations was to be at least 1.5^{o} and sideslip amplitude approximately 5 mm.

(3) With a typical model, the yaw frequency was to be in the range 3 Hz to 5 Hz, with sideslip frequency about 1 Hz higher and roll frequency at least 1 Hz higher than that of sideslip. These frequencies were required to be as low as possible consistent with being controllable without instability of the oscillation.

(4) Under maximum aerodynamic load the unit was required to sustain 18 kN applied at any point ±5 cm from the centre of the front spring.

The unit thus designed is shown in Figs 1 and 2. The model attachment section is rectangular in cross-section and allows space for model accessories on either side inside the model fuselage. The model is secured by six vertical bolts through the attachment section. The front spring has concave vertical surfaces to give sufficient strength and ensure that the roll and yaw frequencies lie within the defined limits. The spring unit design allows for a tensile stress level, due to normal force, of 150 MN/m^2 and an additional alternating stress of ±150 MN/m^2. An alternating shear stress of ±100 MN/m^2 is allowed for the roll oscillation case. Aft of the front spring the cross-section changes from rectangular to circular before a transition to the rear spring which, in combination with the front spring, allows flexibility in sideslip. This spring is made as long as practicable to reduce the sideslip frequency which, as previously indicated, must be lower than the roll frequency to avoid instability of the model during wind-on tests. The cross-section is varied along the length

to give a constant stress level. The male section of a 6 inch Swedish joint is machined onto the rear of the spring unit to allow attachment to the rear sting which is mounted on the wind-tunnel quadrant. The vibration generator and drive system are installed aft of the rear spring and connected to the model attachment section by a rod which passes down a bore hole in the sting. The front and rear springs are strain gauged to allow displacement measurement and also static load measurements of normal force, pitching moment, sideforce, yawing moment and rolling moment.

The spring unit was manufactured from 2½% Ni-Cr steel with an ultimate tensile stress of 900 MN/m^2.

4 DESIGN OF DRIVE SYSTEM

The drive system is shown diagrammatically in Fig 3. The electromagnetic vibration generator applies both a longitudinal force and a rolling torque to the offset arm which is rigidly attached to the model. The longitudinal force produces an internal couple between the model and the end of the sting which is equivalent to a combined external yawing moment and sideforce. The system thus provides yawing, rolling and sideforce excitation at the same time. The bearings shown in Fig 3 are purely diagrammatic: in practice crossed-spring centres are used instead of rotating bearings and parallel flat springs instead of sliding bearings. The ends of links are provided with flat spring flexures in the appropriate planes. There is a PTFE sliding bush situated towards the front of the driving rod but this serves only as a steady and carries very small side loads.

To excite each mode of oscillation the oscillator is set to the appropriate frequency and the current adjusted to give the required amplitude. The excitation will also produce a small response in the other modes which is accounted for in the analysis.

The driving rod is inevitably rather flexible in torsion and this flexibility combined with the internal damping of the vibration generator introduces a troublesome phase difference between the current in the vibration generator and the forces applied to the model. The flexible drive system itself is therefore used as a dynamometer to measure the excitation force. The method is illustrated diagrammatically for a single-degree-of-freedom system in Fig 4. Equation (1) is the equation of motion of the mass in terms of the driving force F. Equation (2) is simply the relation between the force F and the deflection of the driving system. Combining equations (1) and (2) gives equation (3) which is of exactly

the same form as equation (1) but defines a slightly different system in which the drive system stiffness is added to the main stiffness and the driving force is proportional to the vibration generator displacement. The latter is measured in the actual drive system by means of strain gauges on the crossed spring pivots of the main lever shown in Fig 3. With this arrangement, the measured damping does not include the internal damping of the vibration generator; this is important if it is required to measure small values of aerodynamic damping.

During a wind-off oscillation there is very little displacement of the vibration generator armature at or near the resonant frequency since the excitation is in quadrature with the model displacement and the damping is very small. In a wind-on test with high aerodynamic damping there will be large displacements of the vibration generator armature in quadrature with the displacement. The vibration generator has a maximum thrust of 125 N at a stroke of ±6.5 mm and for a maximum roll or yaw deflection of the model of 1.5° the drive system design must satisfy two conditions:

(a) when the model is displaced 1.5° in yaw or roll a force of 125 N must be exerted by the vibration generator to keep the armature in the neutral position,

(b) when the model is held in an undeflected position a force of 125 N must be exerted by the vibration generator to move the armature 6.5 mm.

5 CALIBRATION

Calibration tests are made to determine the static calibration factors of the strain gauge balance and the constants required for working out the results of the dynamic measurements. The dynamic calibrations also verify that the rig behaviour agrees with the assumed equations of motion. The tests made are as follows:

(1) Static calibrations including those for the elimination of balance interactions.

(2) Dynamic calibrations to determine:

(i) Signal proportioning factors e_a and e_b (see Appendix B).

(ii) Strain gauge factors for yaw, sideslip and roll (to convert volts to displacement).

(iii) Strain gauge factors for excitation.

(iv) Model inertias.

A specially designed calibrating frame is used for both static and dynamic calibrations (Fig 5). The frame has provision for the static loading of the balance and for making known inertia changes by adding or transferring 1kg masses. Gross changes in the mass and longitudinal CG position of the frame can be made by means of disc masses attached to the central tube. Thus the mass and inertias of the frame can be adjusted approximately to represent those of the model.

5.1 Static calibrations

The static calibration of the balance is done in the usual way by applying known loads to the calibrating frame to strain the balance in each of the five components: normal force, pitching moment, sideforce, yawing moment and rolling moment. Linear interactions are eliminated by means of a signal mixing unit. When the known load is applied to a given channel, any proportion of that signal can be added to any other channel to cancel the unwanted components.

5.2 Dynamic calibrations

Since the spring system is symmetrical, the roll signal can equally well be used to measure roll displacement. However, because of yaw/sideslip cross stiffness in the system, linear interactions are needed between the yawing moment and sideforce signals to convert them to yaw and sideslip measurements. Special potentiometers are provided in the signal mixing unit for this purpose. The procedure for determining these proportioning factors for angular displacement in yaw and sideways displacement of the model reference in either the A or B modes is described in Appendix B.

Before the model inertias can be measured it is necessary to determine the stiffness of the spring unit and transducer factors for the strain gauges. The mass configurations are chosen so as to enable the primary and cross stiffness of the spring unit to be determined, *eg* the 'yawing' stiffness can be derived by iteration on the input value to obtain the known change in ΔI_{zz} . For each of the nine mass configurations shown in Fig 6 the frame is oscillated in the A, B and C modes. The frequency and the in-phase and in-quadrature components of the yaw, sideslip, roll and excitation signals are recorded in each mode. The frame is oscillated at near resonant frequency so that the excitation terms are negligibly small. The equations of motion for yawing moments used in the analysis of these tests are given in Appendix C. These equations are obtained by re-arranging equations (A-1), (A-2) and (A-3) to determine inertias instead of stiffnesses. Similar equations are used for sideforces and rolling moments.

The measurements and assumed values for the strain gauge factors and stiffnesses are used to solve the equations of motion and obtain the system inertias. The changes in the inertias ΔI_{zz}, ΔI_{xx}, Δm, etc are then compared with the actual changes known to have been made. Using these comparisons as the criterion, the strain gauge factors and stiffnesses are obtained by an iterative trial and error process. A typical set of results from an inertia calibration is given in Table 1 and the iteration procedure is described in Appendix C. Having determined the strain gauge factors and stiffnesses, the model is placed on the sting and a single set of measurements in the A, B and C modes is used to calculate the inertias of the model. In all these inertia tests the frequency is adjusted so that the component of the excitation in phase with the primary displacement is zero and the in-quadrature components are ignored. The resulting errors in the inertia calculations are negligible since system dampings are only about 0.1% of critical.

Using the calibrating frame or model, the inertias of which are known, the excitation measuring system is calibrated by changing the frequency (in each mode) so that relatively large components of the excitation signal in phase with the displacement are introduced. The excitation factors (C_N, C_Y and C_L) are calculated by minimising the change in each of the stiffnesses with frequency. Ideally these changes should be zero.

6 WIND-TUNNEL TESTS

As part of a programme to develop techniques for the investigation of the lateral stability characteristics of swept wing combat aircraft at high subsonic speeds and limiting angle of attack the lateral derivatives of a 0.16 scale model of the Gnat T Mk 1 aircraft were measured in the 8ft × 8ft wind tunnel at RAE Bedford. Tests were made, fin-on and fin-off, at a Reynolds number of 7×10^6, based on $\bar{c}$, compared with the full scale value of 19×10^6. Fin-on tests were made on two separate occasions, referred to as series 1 and 2 in the Figures, and the results from both series of tests, at M = 0.7, are presented. In series 2, tests were made up to higher angles of attack than in series 1.

6.1 Rig and model

The model and sting are shown installed in the tunnel working section in Fig 2. The complete sting can be assembled outside the working section before fitting into the quadrant. The rear part of the sting is joined to the spring unit by a standard 6 inch joint. The vibration generator is mounted above the

rear sting and connected to the drive system on its downstream face. When assembled the sting can be fitted into the quadrant roll gear by means of a standard dog-clutch fitting on the rear sting. The model fuselage is bolted onto the rectangular section attachment block on the spring unit.

A sketch of the model is shown in Fig 7. The rear fuselage was distorted to allow for sufficient clearance between the sting and model at the sting exit point. Air intakes were faired in since there was no allowance for air flow through the model. Remotely controlled tail surfaces were provided to trim out pitching moments. The rear fuselage and wings were manufactured from aluminium alloy, the nose from glass reinforced plastic and the tail surfaces from steel.

No transition fixing was used for these oscillatory tests.

6.2 Results

Because of the kinematic constraints imposed on the motion of the model in these oscillatory tests, certain of the aerodynamic derivatives are measured in combination, as n'_{ψ}, n'_{ϕ} etc. The relations between these derivatives and those usually used in flight dynamics, are given in Table 2. Derivatives are computed with respect to body axes.

The oscillatory measurements are compared with estimates, static wind-tunnel measurements (y_v, n_v and ℓ_v) and flight measurements (y_v, n_v, ℓ_v, n_p and ℓ_p) in Figs 8, 9 and 10. There are some differences in the values of derivatives obtained from the two series of oscillatory tests with fin-on. These differences are an indication of the repeatability of the results using this technique and it may be assumed that at any particular angle of attack the most accurate value of each derivative would be the mean of the two measurements.

Derivatives were estimated using methods given in the Engineering Sciences Data Unit (ESDU) Data Sheets and 'USAF Stability and Control Datcom (DATCOM)'. ESDU methods enabled estimates to be made of n_v, ℓ_v, n_r and ℓ_p. DATCOM contained estimation methods for all the derivatives measured.

The static measurements[2] included in the Figures were made in the RAE 8ft × 8ft wind tunnel using a similar Gnat model which, however, did not have rear-fuselage distortion. Also, the fin-off case quoted for these tests refers to simultaneous removal of both fin and tail, but the absence of the tailplanes on the model with no fin would not be expected in this context, to have any significant effect on y_v and n_v and the effect on ℓ_v would be small. Additionally, transition fixing was employed in these tests.

Flight results shown for y_v, n_v, ℓ_v, n_p and ℓ_p were calculated by 'parameter identification' techniques from records of Dutch Roll oscillations[3].

Estimated aircraft inertias were used in these calculations but the accuracy of the data is expected to be up to the normal standards for this type of experiment.

It has already been noted that in the present tests some derivatives can only be obtained in combination with others, *eg* $\ell_p + \ell_{\dot{v}} \sin\alpha$. These are compared in the figures with the primary derivative in such combinations, *eg* ℓ_p , on the assumption that for the configuration tested and the angle of attack range covered the $\dot{v}$ derivative is negligible.

6.2.1 y_v, n_v and ℓ_v (Fig 8a and b)

The oscillatory test results shown in Fig 8a appear to agree with both static and flight test results except that ℓ_v appears to be about 20% larger than the static value throughout the angle of attack range. There is also less fall-off in $-\ell_v$ at the higher angles of attack. This tendency for the results of oscillatory tests to give numerically smaller ℓ_v values than static tests has been noticed in previous tests where the angles of attack are such that substantial areas of separated flow are present on the wings. It is, thus, considered that this discrepancy is probably due to a genuine difference between static and dynamic flow conditions, although the reasons are not clear. However, there is a consistent difference between the oscillatory tunnel and flight test results, even at low angle of attack, which is harder to explain. Both estimation methods give values of n_v which agree closely with the measurements but the estimates of y_v and ℓ_v are consistently greater, numerically, than the oscillatory test results.

In Fig 8b the contribution of the fin to the sideslip derivatives is examined and good agreement between the contributions obtained from static and oscillatory tests exists generally for y_v and n_v . However, the magnitude of the contribution to ℓ_v is consistently greater for the oscillatory data than for the static data. It is not thought likely that the removal of the tailplane with the fin in the static tests will have affected this comparison. Estimates of the fin effect on y_v and n_v are also in fairly close agreement with the measurements but the fin effect on ℓ_v is consistently overestimated relative to the other data.

6.2.2 $y_r - y_{\dot{v}} \cos\alpha$, $n_r - n_{\dot{v}} \cos\alpha$ and $\ell_r - \ell_{\dot{v}} \cos\alpha$ (Fig 9a and b)

There are noticeable differences between the two series of oscillatory test results for these damping-due-to-rate-of-yaw derivatives as shown in Fig 9a. The largest discrepancy occurs in $y_r - y_{\dot{v}} \cos\alpha$, which is the least significant of the derivatives due to yaw rate and depends on the measurement of a very small in-quadrature signal. The estimated values of y_r and n_r are in general smaller than the measured values but the estimate of ℓ_r is greater.

Fig 9b shows that the fin contribution to these derivatives is in reasonable agreement with the estimated fin-effect. However the fuselage and wing contributions to y_r and n_r appear to be underestimated and their contribution to ℓ_r overestimated with respect to the measured data.

6.2.3 $y_p + y_{\dot{v}} \sin\alpha$, $n_p + n_{\dot{v}} \sin\alpha$ and $\ell_p + \ell_{\dot{v}} \sin\alpha$ (Fig 10a and b)

Comparing the two series of oscillatory test results, Fig 10a shows only small discrepancies in the derivatives $n_p + n_{\dot{v}} \sin\alpha$ and $\ell_p + \ell_{\dot{v}} \sin\alpha$ but a large discrepancy in the values of $y_p + y_{\dot{v}} \sin\alpha$. The estimates of n_p and ℓ_p agree reasonably well with the measurements however, and in the case of y_p the estimates appear to agree well with the results of the series 2 tests. However, no reason can be found for rejecting the series 1 values of $y_p + y_{\dot{v}} \sin\alpha$ and this agreement must be regarded as fortuitous. A possible cause of inaccuracy in the measurement of $y_p + y_{\dot{v}} \sin\alpha$ and $n_p + n_{\dot{v}} \sin\alpha$ will be discussed later in section 7 and Appendix A.

There is fairly good agreement between the tunnel and flight results for n_p and ℓ_p but the scatter in the flight data is considerable. However, there is significant disagreement at low angles-of-attack where the flight value of n_p is more negative than both the result from oscillatory tests and the estimate of this derivative. Flight tests on the Gnat aircraft[3] have shown that at M = 0.7, onset of wing rock occurs at $\alpha \doteq 9^\circ$. This correlates with the marked reduction in the roll damping derivative, $\ell_p + \ell_{\dot{v}} \sin\alpha$ between $\alpha = 8.5^\circ$ and 10.5° measured in the tunnel.

As shown in Fig 10b the fin effect measured in the series 2 tests is negligible. This agrees with the estimated small or zero effects for these derivatives.

6.2.4 Effective fin moment-arm

The yawing moment/sideforce and rolling moment/sideforce ratios of the fin contribution due to sideslip, $(\Delta n_v/\Delta y_v)$ and $(\Delta \ell_v/\Delta y_v)$, and due to yaw rate, $(\Delta n_r/\Delta y_r)$ and $(\Delta \ell_r/\Delta y_r)$, are plotted against angle of attack in Fig 11. The fin contributions to the derivatives due to roll rate are negligible as shown in section 6.2.3 and have not been included.

The yawing moment/sideforce ratio is a measure of the effective fin-arm along the longitudinal axis in terms of reference wing span b. Similarly, the rolling moment/sideforce ratio is a measure of the effective fin-arm along a normal axis. From Fig 11 it is evident that reasonable values of effective fin

moment-arm are derived from the test results and they agree fairly closely with those derived from the estimated derivatives. It should be noted that for a conventional fin with a centre of pressure above and behind the moment reference centre, a positive sideforce causes a positive rolling moment and a negative yawing moment when referred to geometric body axes.

7 FUTURE DEVELOPMENTS

7.1 Modification to drive system

In the present drive system all three modes of oscillation are excited by the same mechanical components. The linkage is arranged to apply simultaneously rolling or fore and aft (for yaw and sideslip) excitation to the model. A particular mode of oscillation is excited by tuning at the appropriate frequency. In a wind-on test the rolling mode is usually heavily damped and near maximum excitation power is used to obtain the required amplitude of oscillation. This means that besides a large in-quadrature roll excitation force, large in-quadrature yaw and sideslip components are also being fed in by the excitation system at the roll frequency. These components cause most of the yawing and sideslipping response measured and the responses due to aerodynamic excitation are masked. Thus the derivatives $y_p + y_{\dot{v}} \sin\alpha$ and $n_p + n_{\dot{v}} \sin\alpha$ are measured mainly as the difference of two large quantities, the mechanical excitation and the response, which results in poor accuracy. Examples of actual measurements are given in Table 3. The major contributions to $N_{\dot{\psi}}$ wind-on, are two terms of the same sign, $N_{\dot{y}}\left(\frac{y}{\psi}\cos\varepsilon_1\right)_a$ and $\frac{1}{\omega_a}\left(\frac{N_e}{\psi}\sin\varepsilon_3\right)_a$ whereas the wind-on value of $N_{\dot{\phi}}$ is small compared with the two components $\omega_c\left(\frac{\psi}{\phi}\sin\varepsilon_1\right)_c I_{zz}$ and $\frac{1}{\omega_c}\left(\frac{N_e}{\phi}\sin\varepsilon_3\right)_c$ of opposite sign which derive from yawing excitation in the rolling mode.

By the introduction of two nominally independent drive systems, one to excite roll and the other to excite yaw and sideslip it is hoped to increase the accuracy of measurement of the derivatives due to rate of roll. The proposed arrangement is shown schematically in Fig 12. Both systems will excite the model through the same driving rod, similar to that used at present, and utilise a common vibration generator. During a roll mode the yaw/sideslip excitation system will be clamped to earth at the connection to the vibration generator and similarly the roll system will be clamped during a yaw or sideslip mode. It is proposed that the clamping and connection operations will be under remote control so that no interruption of the test will be necessary.

7.2 Tests at limiting angles of attack

The present straight sting allows testing up to an angle of attack up to $22\frac{1}{2}^{\circ}$ in the 8ft × 8ft wind tunnel. A new cranked-sting section is being designed to fit between the 6 inch joint of the spring unit and the quadrant which will allow tests to be made over an extended range of angle of attack (up to 40°) at Reynolds numbers of about one third the full scale value for a typical combat aircraft.

8 CONCLUSIONS

A rig has been developed to measure the oscillatory lateral aerodynamic derivatives of wind-tunnel models over the full operating range of the 8ft × 8ft wind tunnel at RAE Bedford. Tests can be made up to limiting angles of attack at Reynolds numbers of about one third the full scale value of a typical combat aircraft.

Measurements made on a 0.16 scale model of a Gnat aircraft, fin-on and fin-off, have been compared, at a Mach number of 0.7, with flight test results, wind-tunnel static test results and with estimates. In general, agreement with these other data is reasonably good but the accuracy of measurement of some of the cross-damping derivatives, such as sideforce-due-to-rate-of-roll, is not up to the desired level. A re-design of the drive system is proposed to improve accuracy in this respect.

This facility enables lateral derivatives to be measured on models of new aircraft configurations during the design stage. These derivatives may be used to assist the prediction of dynamic phenomena of various kinds which may result in limitations to the flight envelope. As an example of this, the reduction in roll damping measured in the present tests on a model of the Gnat aircraft at $M = 0.7$, $\alpha \doteq 9^{\circ}$ has been correlated with the onset of wing rock measured in flight.

Appendix A

EQUATIONS OF MOTION

The following equations of motion define a system with three degrees of freedom and apply to yawing moments, sideforces and rolling moments respectively.

$$(\omega^2 I_{zz} + i\omega N_{\dot{\psi}} + N_{\psi})\psi + (\omega^2 m\bar{x} + i\omega N_{\dot{y}} + N_y)y + (-\omega^2 I_{zx} + i\omega N_{\dot{\phi}} + N_{\phi})\phi + N_e = 0 \quad \ldots\ldots \text{(A-1)}$$

$$(\omega^2 m\bar{x} + i\omega Y_{\dot{\psi}} + Y_{\psi})\psi + (\omega^2 m + i\omega Y_{\dot{y}} + Y_y)y + (-\omega^2 m\bar{z} + i\omega Y_{\dot{\phi}})\phi + y_e = 0 \quad \text{(A-2)}$$

$$(-\omega^2 I_{zx} + i\omega L_{\dot{\psi}} + L_{\psi})\psi + (-\omega^2 m\bar{z} + i\omega L_{\dot{y}} + L_y)y = (\omega^2 I_{xx} + i\omega L_{\dot{\phi}} + L_{\phi})\phi + L_e = 0. \quad \ldots\ldots \text{(A-3)}$$

The symbols are defined as follows:

Axes:

All forces, moments and displacements are referred to a system of earth axes fixed in the mean position of the oscillating model.

Displacements and velocities:

ψ $\dot{\psi}$ yawing

y $\dot{y}$ sideslipping

ϕ $\dot{\phi}$ rolling

Inertias:

m mass

$\bar{x}$, $\bar{z}$ coordinates of CG

Inertias:

I_{xx} roll inertia

I_{zz} yaw inertia

I_{xz} cross inertia

Forces and moments:

N yawing moment

Y side force

L rolling moment

Derivatives are denoted by suffices, *eg*

$$N_{\psi} = \partial N/\partial\psi$$

ω is the circular frequency and the suffix e denotes an excitation force or moment.

Each of the above equations contains six unknown derivatives and in the tunnel experiment separate measurements are made in the yawing, sideslipping and rolling modes. These will be referred to as A, B and C respectively. It is convenient to divide the equations by ψ for A mode tests, by y for B mode tests and ϕ for C mode tests and the complex equations are split into real and imaginary parts to provide six equations for determining the six unknowns. If ε_1 and ε_2 are the phase differences between the primary signal (*eg* the 'yaw' signal in the A mode) and the other signals in any particular mode, then for example the six yawing moment equations used to determine the six yawing moment derivatives, may be written:

$$N_{\psi} = -\omega_a^2\left[I_{zz} + \left(\frac{y}{\psi}\cos\varepsilon_1\right)_a m\bar{x} - \left(\frac{\phi}{\psi}\cos\varepsilon_2\right)_a I_{zx}\right] + \omega_a\left[\left(\frac{y}{\psi}\sin\varepsilon_1\right)_a N_{\dot{y}} + \left(\frac{\phi}{\psi}\sin\varepsilon_2\right)_a N_{\dot{\phi}}\right] - \left[\left(\frac{y}{\psi}\cos\varepsilon_1\right)_a N_y + \left(\frac{\phi}{\psi}\cos\varepsilon_2\right)_a N_{\phi} + \left(\frac{N_e}{\psi}\cos\varepsilon_3\right)_a\right] \quad (A\text{-}1)$$

$$N_y = -\omega_b^2\left[m\bar{x} - \left(\frac{\phi}{y}\cos\varepsilon_1\right)_b I_{zx} + \left(\frac{\psi}{y}\cos\varepsilon_2\right)_b I_{zz}\right] + \omega_b\left[\left(\frac{\phi}{y}\sin\varepsilon_1\right)_b N_{\dot{\phi}} + \left(\frac{\psi}{y}\sin\varepsilon_2\right)_b N_{\dot{\psi}}\right] - \left[\left(\frac{\phi}{y}\cos\varepsilon_1\right)_b N_{\phi} + \left(\frac{\psi}{y}\cos\varepsilon_2\right)_b N_{\psi} + \left(\frac{N_e}{y}\cos\varepsilon_3\right)_b\right] \quad (A\text{-}2)$$

$$N_{\phi} = -\omega_c^2\left[-I_{zx} + \left(\frac{\psi}{\phi}\cos\varepsilon_1\right)_c I_{zz} + \left(\frac{y}{\phi}\cos\varepsilon_2\right)_c m\bar{x}\right] + \omega_c\left[\left(\frac{\psi}{\phi}\sin\varepsilon_1\right)_c N_{\dot{\psi}} + \left(\frac{\psi}{\phi}\sin\varepsilon_2\right)_c N_{\dot{y}}\right] - \left[\left(\frac{\psi}{\phi}\cos\varepsilon_1\right)_c N_{\psi} + \left(\frac{y}{\phi}\cos\varepsilon_2\right)_c N_y + \left(\frac{N_e}{\phi}\cos\varepsilon_3\right)_c\right] \quad (A\text{-}3)$$

$$N_{\dot{\psi}} = -\omega_a\left[\left(\frac{y}{\psi}\sin\varepsilon_1\right)_a m\bar{x} - \left(\frac{\phi}{\psi}\sin\varepsilon_2\right)_a I_{zx}\right] - \left[\left(\frac{y}{\psi}\cos\varepsilon_1\right)_a N_{\dot{y}} + \left(\frac{\phi}{\psi}\cos\varepsilon_2\right)_a N_{\dot{\phi}}\right] - \frac{1}{\omega_a}\left[\left(\frac{y}{\psi}\sin\varepsilon_1\right)_a N_y + \left(\frac{\phi}{\psi}\sin\varepsilon_2\right)_a N_{\phi} + \left(\frac{N_e}{\psi}\sin\varepsilon_3\right)_a\right] \quad (A\text{-}4)$$

$$N_{\dot{y}} = -\omega_b\left[-\left(\frac{\phi}{y}\sin\varepsilon_1\right)_b I_{zx} + \left(\frac{\psi}{y}\sin\varepsilon_2\right)_b I_{zz}\right] - \left[\left(\frac{\phi}{y}\cos\varepsilon_1\right)_b N_{\dot{\phi}} + \left(\frac{\psi}{y}\cos\varepsilon_2\right)_b N_{\dot{\psi}}\right] - \frac{1}{\omega_b}\left[\left(\frac{\phi}{y}\sin\varepsilon_1\right)_b N_{\phi} + \left(\frac{\psi}{y}\sin\varepsilon_2\right)_b N_{\psi} + \left(\frac{N_e}{y}\sin\varepsilon_3\right)_b\right] \quad (A\text{-}5)$$

$$N_{\dot{\phi}} = -\omega_c\left[\left(\frac{\psi}{\phi}\sin\varepsilon_1\right)_c I_{zz} + \left(\frac{y}{\phi}\sin\varepsilon_2\right)_c m\bar{x}\right] - \left[\left(\frac{\psi}{\phi}\cos\varepsilon_1\right)_c N_{\dot{\psi}} + \left(\frac{y}{\phi}\cos\varepsilon_2\right)_c N_{\dot{y}}\right] - \frac{1}{\omega_c}\left[\left(\frac{\psi}{\phi}\sin\varepsilon_1\right)_c N_{\psi} + \left(\frac{y}{\phi}\sin\varepsilon_2\right)_c N_y + \left(\frac{N_e}{\phi}\sin\varepsilon_3\right)_c\right]. \quad (A\text{-}6)$$

The inertias are obtained from previous calibrations, the frequencies are measured directly and the strain gauge and excitation signals together with the necessary transducer factors, give the vector ratios such as $\left(\frac{y}{\psi} \cos \varepsilon_1\right)_a$ and $\left(\frac{N_e}{\psi} \cos \varepsilon_3\right)_a$. It is assumed that the aerodynamic derivatives are given by the differences between the values measured wind-on and wind-off.

Appendix B

DETERMINATION OF PROPORTIONING FACTORS e_a AND e_b

Because of the yaw/sideslip cross stiffness (see section 5.2), the angular deflection in yaw, ψ, or the sideways displacement of the reference, y, are given by the equations

$$\psi - e_a y = c_a(S_\psi + k_1 S_y) \tag{B-1}$$

$$y - e_b \psi = c_b(S_y + k_2 S_\psi) \tag{B-2}$$

The angular deflection in roll, ϕ is given by

$$\phi = c_c S_\phi \tag{B-3}$$

where e_a and e_b are proportioning factors in rad/m and m/rad respectively

c_a, c_b and c_c are the yaw, sideways displacement and roll conversion constants in rad/V, m/V and rad/V respectively

S_ψ, S_y and S_ϕ are the signals from the yaw, sideways displacement and roll strain gauges respectively in volts, k_1 and k_2 are potentiometer settings.

Dividing (B-1) by (B-2) and re-arranging gives

$$\frac{y}{\psi} = \frac{e_b + \left(\frac{S_y + k_2 S_\psi}{S_\psi + k_1 S_y}\right)\frac{c_b}{c_a}}{1 + \left(\frac{S_y + k_2 S_\psi}{S_\psi + k_1 S_y}\right)\frac{c_b}{c_a} e_a} \tag{B-4}$$

and similarly dividing (B-2) by (B-1),

$$\frac{\psi}{y} = \frac{e_a + \left(\frac{S_\psi + k_1 S_y}{S_y + k_2 S_\psi}\right)\frac{c_a}{c_b}}{1 + \left(\frac{S_\psi + k_1 S_y}{S_y + k_2 S_\psi}\right)\frac{c_a}{c_b} e_b} \quad . \tag{B-5}$$

If x_a and x_b are the distances of the oscillation axes from the reference in the A and B modes respectively then $\frac{y}{\psi} = x_a$ and $\frac{\psi}{y} = \frac{1}{x_b}$. If $(S_y + k_2 S_\psi) = 0$ in (B-4) then $e_b = x_a$ and if $(S_\psi + k_1 S_y) = 0$ in (B-5), $e_a = \frac{1}{x_b}$. In the A mode k_2 is adjusted so that $(S_y + k_2 S_\psi) = 0$ and in the B mode k_1 is adjusted so that $(S_\psi + k_1 S_y) = 0$. e_a and e_b can then be determined by locating the oscillation axes in the A and B modes. This procedure is carried out using the calibrating frame loaded to simulate approximately the inertia of the model to be tested.

Appendix C

ANALYSIS OF INERTIA CALIBRATIONS

The equations of motion, (A-1) to (A-3) given in Appendix A can be re-written in terms of inertias:

$$I_{zz} = -\frac{1}{\omega_a^2}\left[N_\psi + \left(\frac{y}{\psi}\cos\varepsilon_1\right)_a N_y + \left(\frac{\phi}{\psi}\cos\varepsilon_2\right)_a N_\phi + \left(\frac{N_e}{\psi}\cos\varepsilon_3\right)_a\right]$$

$$+\frac{1}{\omega_a}\left[\left(\frac{y}{\psi}\sin\varepsilon_1\right)_a N_{\dot{y}} + \left(\frac{\phi}{\psi}\sin\varepsilon_2\right)_a N_{\dot{\phi}}\right]$$

$$-\left[\left(\frac{y}{\psi}\cos\varepsilon_1\right)_a m\ddot{\bar{x}} - \left(\frac{\phi}{\psi}\cos\varepsilon_2\right)_a I_{zx}\right]$$

$$m\ddot{\bar{x}} = -\frac{1}{\omega_b^2}\left[N_y + \left(\frac{\phi}{y}\cos\varepsilon_1\right)_b N_\phi + \left(\frac{\psi}{y}\cos\varepsilon_2\right)_b N_\psi + \left(\frac{N_e}{y}\cos\varepsilon_3\right)_b\right]$$

$$+\frac{1}{\omega_b}\left[\left(\frac{\phi}{y}\sin\varepsilon_1\right)_b N_{\dot{\phi}} + \left(\frac{\psi}{y}\sin\varepsilon_2\right)_b N_{\dot{\psi}}\right]$$

$$-\left[-\left(\frac{\phi}{y}\cos\varepsilon_1\right)_b I_{zx} + \left(\frac{\psi}{y}\cos\varepsilon_2\right)_b I_{zz}\right]$$

$$-I_{zx} = -\frac{1}{\omega_c^2}\left[N_\phi + \left(\frac{\psi}{\phi}\cos\varepsilon_1\right)_c N_\psi + \left(\frac{y}{\phi}\cos\varepsilon_2\right)_c N_y + \left(\frac{N_e}{\phi}\cos\varepsilon_3\right)_c\right]$$

$$+\frac{1}{\omega_c}\left[\left(\frac{\psi}{\phi}\sin\varepsilon_1\right)_c N_{\dot{\psi}} + \left(\frac{y}{\phi}\sin\varepsilon_2\right)_c N_{\dot{y}}\right]$$

$$-\left[\left(\frac{\psi}{\phi}\cos\varepsilon_1\right)_c I_{zz} + \left(\frac{y}{\phi}\cos\varepsilon_2\right)_c m\ddot{\bar{x}}\right]$$

and similarly for sideforces and rolling moments. The equations for damping derivatives, (A-4) to (A-6) remain unchanged.

If R_1 and R_2, R_3 and R_4, R_5 and R_6, R_7 and R_8 are phase and quadrature components of the yaw, excitation, sideslip and roll signals respectively in the A mode, then:

ΔI_{zz} = 6.0158 kg m^2 = change in yawing moment of inertia between configurations 1 and 2

Δm = 24 kg = change in mass between configurations 1 and 2

ΔI_{xx} = 2.7258 kg m^2 = change in rolling moment of inertia between configurations 1 and 2

$\Delta m\bar{x}_1$ = 12 kg m = change in yaw/sideways displacement inertia coupling between configurations 3 and 4 obtained from B mode

$\Delta m\bar{x}_2$ = 12 kg m = change in yaw/sideways displacement inertia coupling between configurations 3 and 4 obtained from A mode

ΔI_{xz_1} = 3.9 kg m^2 = change in yaw/roll inertia coupling between configurations 6 and 7 obtained from C mode

ΔI_{xz_3} = 3.9 kg m^2 = change in yaw/roll inertia coupling between configurations 6 and 7 obtained from A mode

$\Delta m\bar{z}_2$ = 7.8 kg m = change in roll/sideways displacement inertia coupling between configurations 8 and 9 obtained from C mode

$\Delta m\bar{z}_3$ = 7.8 kg m = change in roll/sideways displacement inertia coupling between configurations 8 and 9 obtained from B mode.

$m\bar{x}_1$ and $m\bar{x}_2$, I_{xz_1} and I_{xz_3}, $m\bar{z}_2$ and $m\bar{z}_3$ are the yaw/sideways displacement, yaw/roll and roll/sideways displacement couplings for configuration 5. $m\bar{x}_1 = m\bar{x}_2 = -1$ kg m. I_{xz_1} and I_{xz_3}, $m\bar{z}_2$ and $m\bar{z}_3$ are nominally zero.

Iteration procedure (compute inertia changes between each stage):

1 Estimate values for system stiffnesses, strain gauge conversion constants and, using values of e_a and e_b previously determined, compute inertia changes.

2 Adjust primary stiffnesses to correct ΔI_{zz}, Δm and ΔI_{xx}.

3 Adjust conversion constants c_a, c_b and c_c to correct $\Delta m\bar{x}$, ΔI_{xz} and $\Delta m\bar{z}$.

4 Adjust cross stiffnesses to correct $m\bar{x}$, I_{xz} and $m\bar{z}$ for configuration 5.

5 If necessary return to stage 2.

6 If necessary make small adjustments to e_a and e_b consistent with accuracy of initial measurement.

Table 1

RESULTS FROM INERTIA CALIBRATIONS - FINAL ITERATION

Configurations	A mode I_1		B mode I_2		C mode I_3	
Yawing moments						
1	11.770	ΔI_{zz} = 6.029 kg m^2	-0.893		-0.115	
2	17.799	(6.0158)*	-1.129		-0.195	
3	14.732		-7.018	$\Delta m\bar{x}_1$ = 12.134 kg m	-0.183	
4	14.836		5.116	(12.0)*	-0.127	
5	14.788		-1.005 $m\bar{x}_1$		-0.159 I_{xz_1}	
6	14.797		-1.003		-2.106	ΔI_{xz_1} = 3.884 kg m^2
7	14.771		-1.000		1.778	(3.9)*
8	14.794		-0.912		-0.021	
9	14.782		-0.983		-0.292	
Sideforces						
1	-0.940		99.297	Δm = 23.963 kg	0.073	
2	-1.118		123.260	(24.0)*	0.113	
3	-6.975	$\Delta m\bar{x}_2$ = 11.860 kg m	111.778		0.160	
4	4.885	(12.0)*	110.868		0.033	
5	-1.019 $m\bar{x}_2$		111.276		0.089 $m\bar{z}_2$	
6	-1.022		111.344		0.158	
7	-1.005		111.316		0.012	
8	-1.006		111.203		-3.854	$\Delta m\bar{z}_2$ = 7.921 kg m
9	-1.014		111.297		4.067	(7.8)*
Rolling moments						
1	-0.195		0.025		3.924	ΔI_{xx} = 2.727 kg m^2
2	-0.324		0.061		6.651	(2.7258)*
3	-0.293		0.191		5.298	
4	-0.221		-0.079		5.282	
5	-0.252 I_{xz_3}		0.057 $m\bar{z}_3$		5.288	
6	-2.213	ΔI_{xz_3} = 3.928 kg m^2	0.112		5.339	
7	1.715	(3.9)*	-0.035		5.239	
8	-0.252		-3.899	$\Delta m\bar{z}_3$ = 7.948 kg m	5.277	
9	-0.247		4.049	(7.8)*	5.316	

* Actual change in inertia given in brackets

Table 2

DEFINITION OF DERIVATIVES

$$-n_v \cos\alpha = n_\psi = \frac{N_\psi}{\frac{1}{2}\rho V^2 Sb}$$

$$-y_v \cos\alpha = y_\psi = \frac{Y_\psi}{\frac{1}{2}\rho V^2 S}$$

$$-\ell_v \cos\alpha = \dot{\ell}_\psi = \frac{L_\psi}{\frac{1}{2}\rho V^2 Sb}$$

$$n_r - n_{\dot{v}} \cos\alpha = n_{\dot{\psi}} = \frac{N_{\dot{\psi}}}{\frac{1}{2}\rho VSb^2}$$

$$n_p + n_{\dot{v}} \sin\alpha = n_{\dot{\phi}} = \frac{\dot{\phi}}{\frac{1}{2}\rho VSb^2}$$

$$y_r - y_{\dot{v}} \cos\alpha = y_{\dot{\psi}} = \frac{Y_{\dot{\psi}}}{\frac{1}{2}\rho VSb}$$

$$y_p + y_{\dot{v}} \sin\alpha = y_{\dot{\phi}} = \frac{Y_{\dot{\phi}}}{\frac{1}{2}\rho VSb}$$

$$\ell_r - \ell_{\dot{v}} \cos\alpha = \ell_{\dot{\psi}} = \frac{L_{\dot{\psi}}}{\frac{1}{2}\rho VSb^2}$$

$$\ell_p + \ell_{\dot{v}} \sin\alpha = \ell_{\dot{\phi}} = \frac{L_{\dot{\phi}}}{\frac{1}{2}\rho VSb^2}$$

Table 3

TYPICAL COMPONENTS OF $N_{\dot{\psi}}$ AND $N_{\dot{\phi}}$

$$N_{\dot{\psi}} = -\omega_a m\bar{x}\left(\frac{y}{\psi}\sin\varepsilon_1\right)_a + \omega_a I_{zx}\left(\frac{\phi}{\psi}\sin\varepsilon_2\right)_a - N_{\dot{y}}\left(\frac{y}{\psi}\cos\varepsilon_1\right)_a - N_{\dot{\phi}}\left(\frac{\phi}{\psi}\cos\varepsilon_2\right)_a - \frac{N_y}{\omega_a}\left(\frac{y}{\psi}\sin\varepsilon_1\right)_a - \frac{N_\phi}{\omega_a}\left(\frac{\phi}{\psi}\sin\varepsilon_2\right) - \frac{1}{\omega_a}\left(\frac{N_e}{\psi}\sin\varepsilon_3\right)_a$$

wind-off	0.50	0.14	-0.03	0.15	0	-0.31	-0.02	0.57
wind-on	14.00	0.71	-0.38	6.13	0.10	-1.44	-0.44	9.31

$$N_{\dot{\phi}} = -\omega_c I_{zz}\left(\frac{\psi}{\phi}\sin\varepsilon_1\right)_c - \omega_c m\bar{x}\left(\frac{y}{\phi}\sin\varepsilon_2\right)_c - N_{\dot{\psi}}\left(\frac{\psi}{\phi}\cos\varepsilon_1\right)_c - N_{\dot{y}}\left(\frac{y}{\phi}\cos\varepsilon_2\right)_c - \frac{N_\psi}{\omega_c}\left(\frac{\psi}{\phi}\sin\varepsilon_1\right)_c - \frac{N_y}{\omega_c}\left(\frac{y}{\phi}\sin\varepsilon_2\right)_c - \frac{1}{\omega_c}\left(\frac{N_e}{\phi}\sin\varepsilon_3\right)_c$$

wind-off	-0.02	-2.5	0.6	-0.03	-0.02	0.35	-0.17	1.79
wind-on	1.37	-26.45	1.68	-0.98	-0.26	4.33	-0.45	23.50

LIST OF SYMBOLS

A	'yawing' mode
b	wing span
B	'sideslipping' mode
C	'rolling' mode
c_a	yaw strain gauge conversion constant
c_b	sideways displacement strain gauge conversion constant
c_c	roll strain gauge conversion constant
C_N	excitation/yaw conversion constant
C_Y	excitation/sideways displacement conversion constant
C_L	excitation/roll conversion constant
$\bar{c}$	geometric mean chord
e_a	proportioning factor (rad/m)
e_b	proportioning factor (m/rad)
i	$\sqrt{-1}$
I_{xx}	rolling moment of inertia
I_{zx}	yaw/roll inertia coupling
I_{zz}	yawing moment of inertia
k_1	potentiometer setting for proportioning sideways displacement signal
k_2	potentioneter setting for proportioning yaw signal
L	rolling moment
L_e	rolling moment applied by excitation system
ℓ (with suffix)	non-dimensional rolling moment
M	Mach number
$m\bar{x}$	yaw/sideways displacement inertia coupling
$m\bar{z}$	roll/sideways displacement inertia coupling
N	yawing moment
N_e	yawing moment applied by excitation system
n (with suffix)	non-dimensional yawing moment derivative
p	angular velocity in roll
R_1 to R_8	in-phase and in-quadrature components of strain gauge signals
r	angular velocity in yaw
S	wing area
S_y	sideways displacement signal (volts)
S_ψ	yawing signal (volts)
V	free stream velocity
v	sideslip velocity

LIST OF SYMBOLS (concluded)

Y	sideforce
Y_e	sideforce applied by excitation system
y	sideways displacement
y (with suffix)	non-dimensional sideforce derivative
α	angle of attack of horizontal fuselage datum
Δ	prefix, to indicate change in inertia or fin contribution to derivative
$\epsilon_1, \epsilon_2, \epsilon_3$	phase angles between component signals and primary signals
ρ	air density
ϕ	angular displacement in roll
ψ	angular displacement in yaw
ω_a	angular frequency of yawing mode
ω_b	angular frequency of sideslipping mode
ω_c	angular frequency of rolling mode

Suffix

p
r
v
y
ϕ
ψ

} denote derivatives with respect to these variables

REFERENCES

No.	Author	Title, etc
1	J.S. Thompson R.A. Fail J.V. Inglesby	Low speed wind-tunnel measurements of the oscillatory lateral stability derivatives for a model of a slender aircraft (HP 115) including the effects of frequency parameter. ARC CP No.1097 (1969)
2	P.J. Haynes	RAE Unpublished Report
3	A. Jean Ross G.W. Foster T. Turvey	An investigation of Dutch roll and wing rock oscillation of a Gnat trainer aircraft: flight test and linear analysis. RAE Technical Report 78032 (1978)

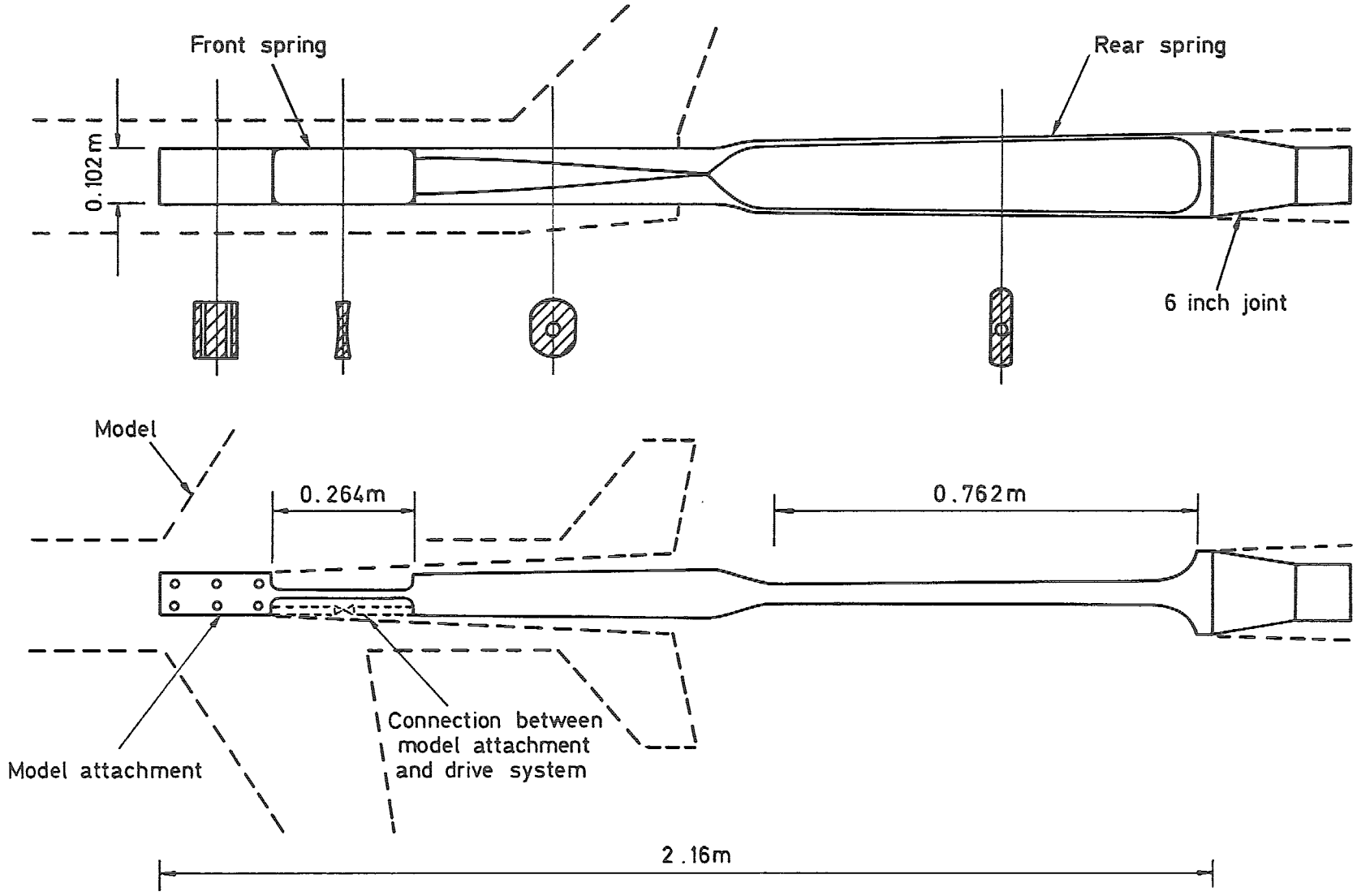

Fig 1 Sketch of spring unit

Fig 1

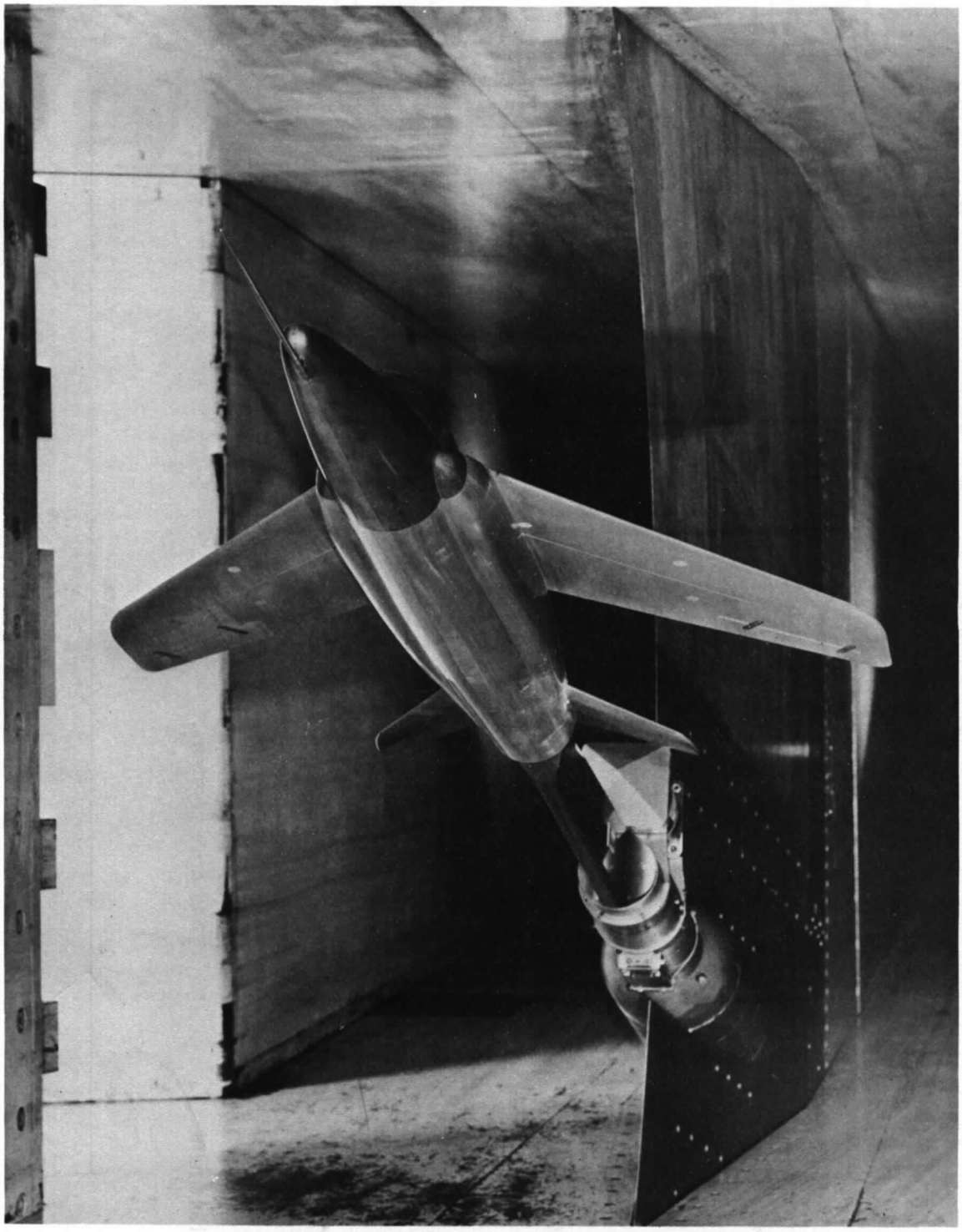

Fig 2 Model and rig installed in 8 ft x 8 ft tunnel working section

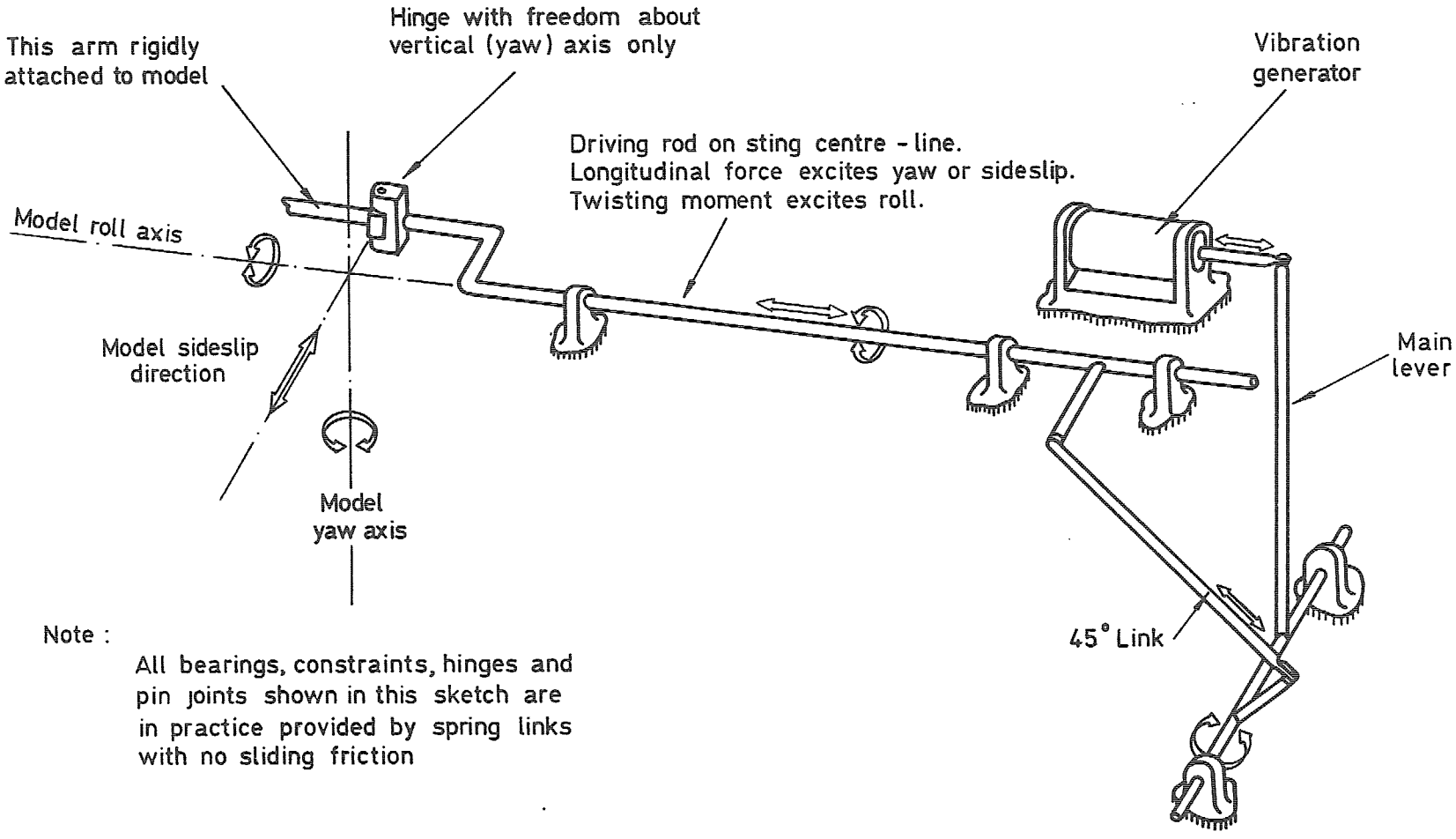

Fig 3 Diagrammatic sketch of excitation system

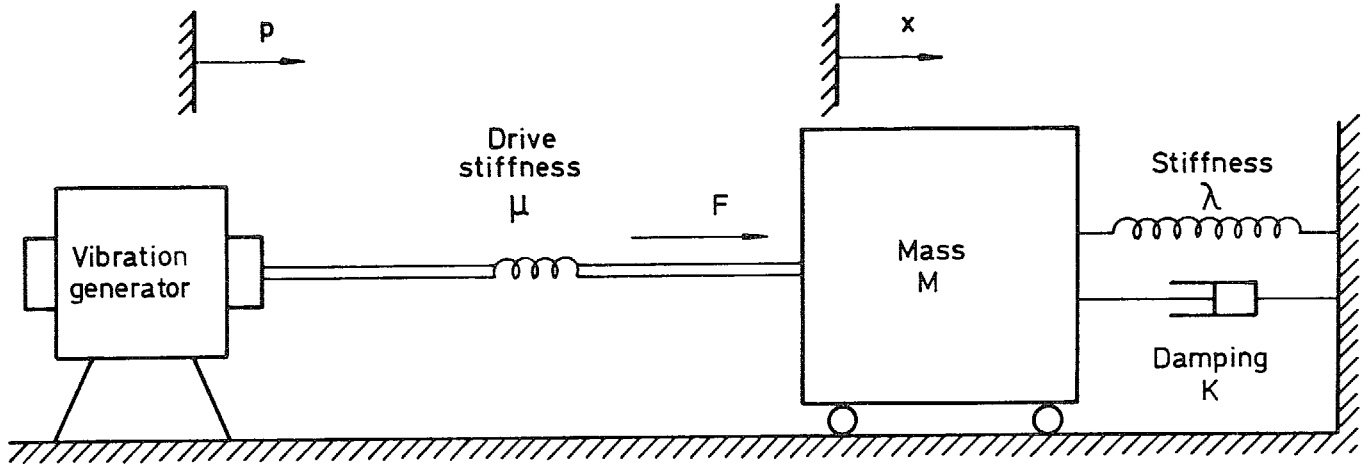

p and x are the displacements of the vibration generator and the mass from their equilibrium positions, F is the driving force

$$[\omega^2 M + j\omega K + \lambda] \; x + F = 0 \quad (1)$$

$$\mu (p - x) + F = 0 \quad (2)$$

$$[\omega^2 M + j\omega K + (\lambda + \mu)] \; x - \mu p = 0 \quad (3)$$

Fig 4 Excitation measurement

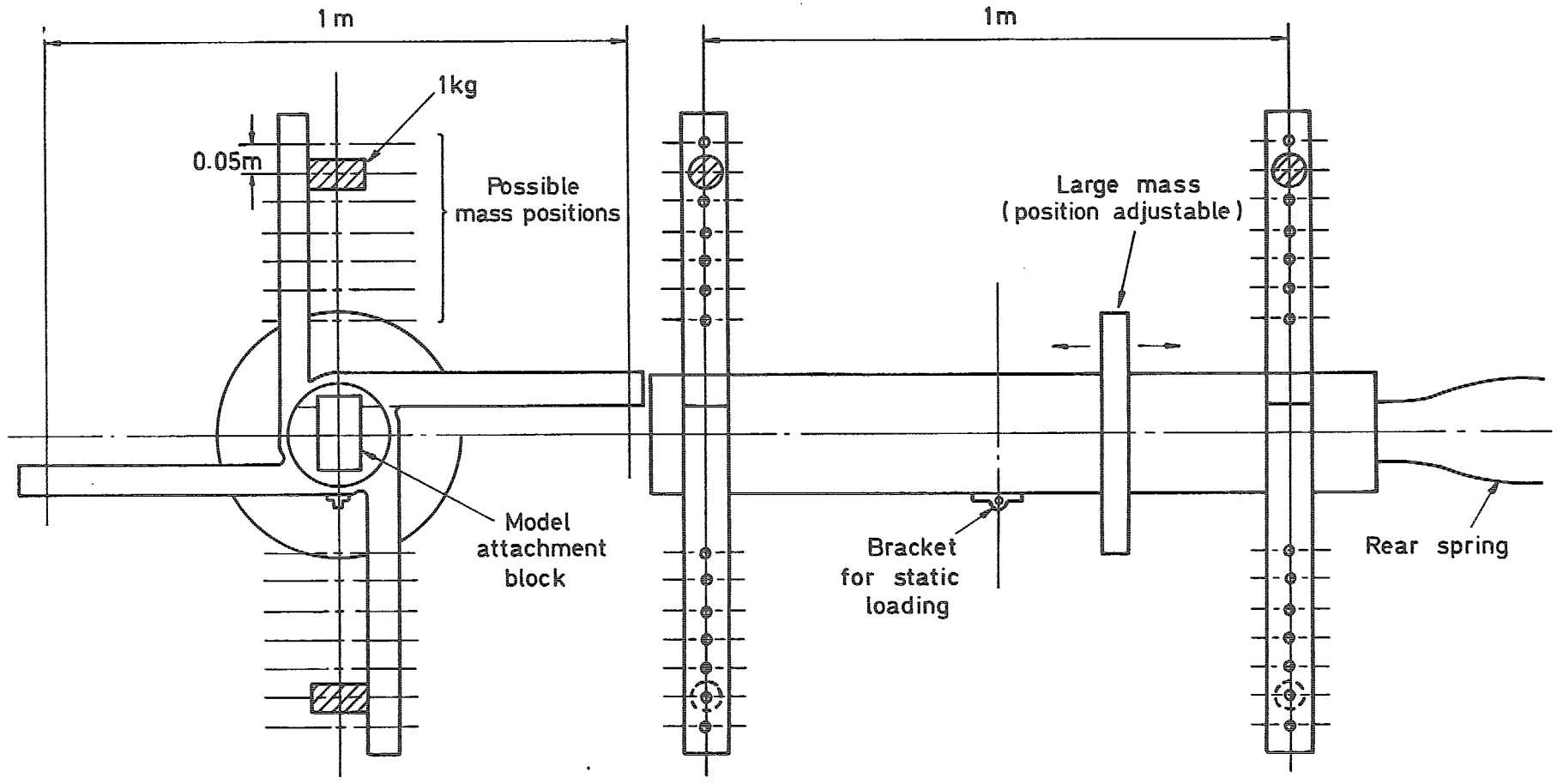

Fig 5 Calibrating frame

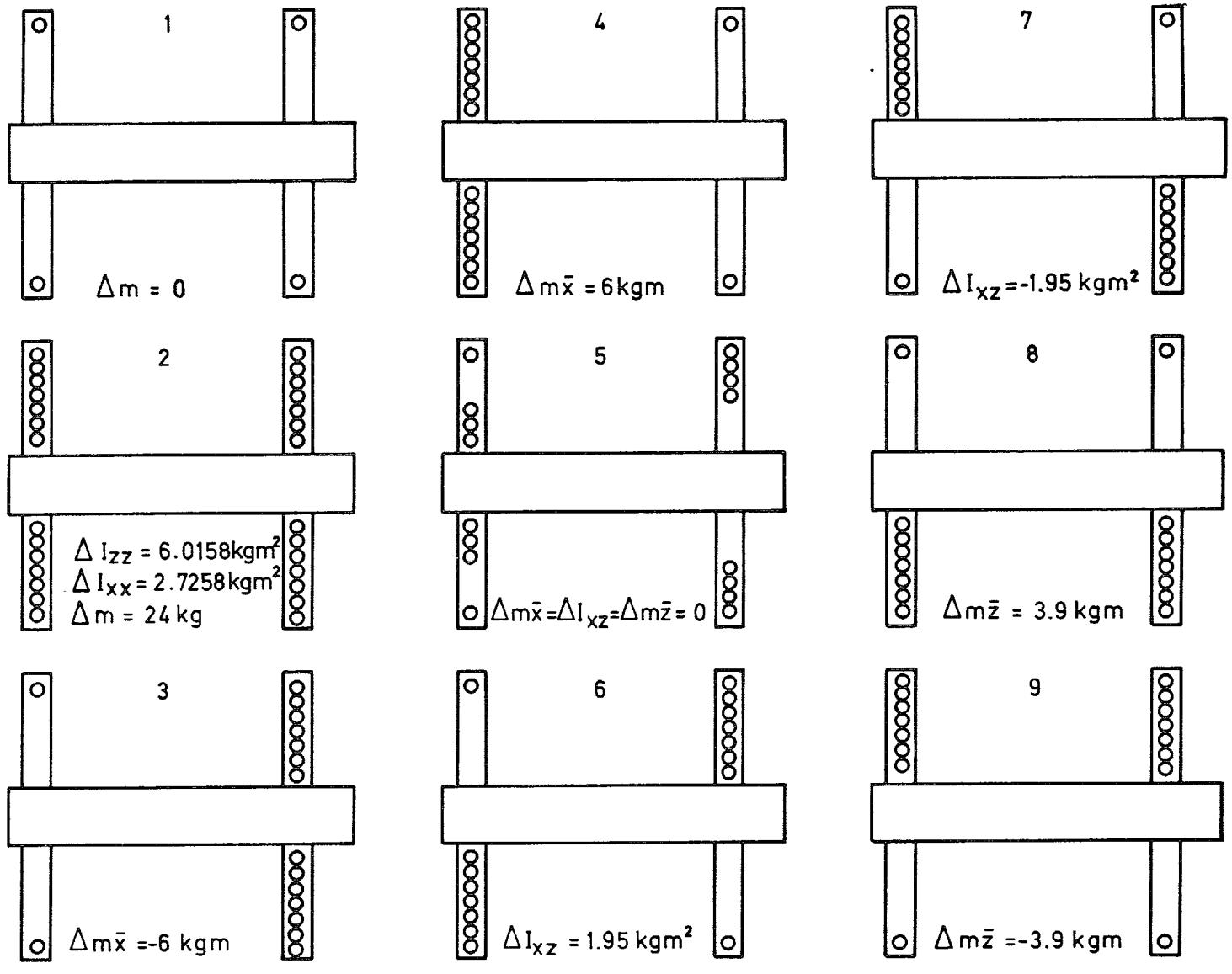

Fig 6 Mass configurations used for the inertia calibrations (see section 5.2)

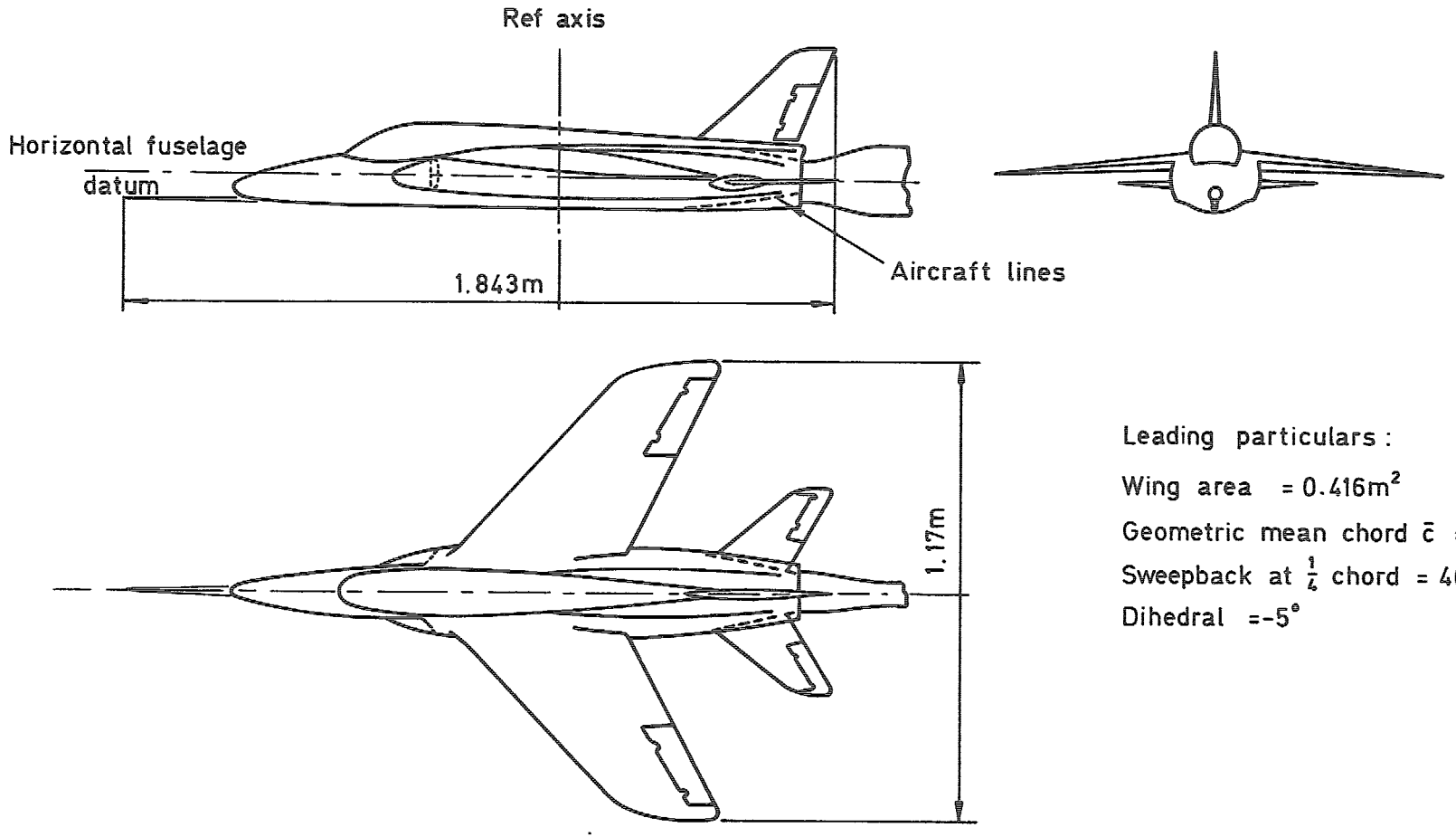

Leading particulars :

Wing area = $0.416m^2$

Geometric mean chord $\bar{c}$ = 0.357m

Sweepback at $\frac{1}{4}$ chord = 40°

Dihedral = -5°

Fig 7 Sketch of Gnat T Mk 1 model

Fig 8 a

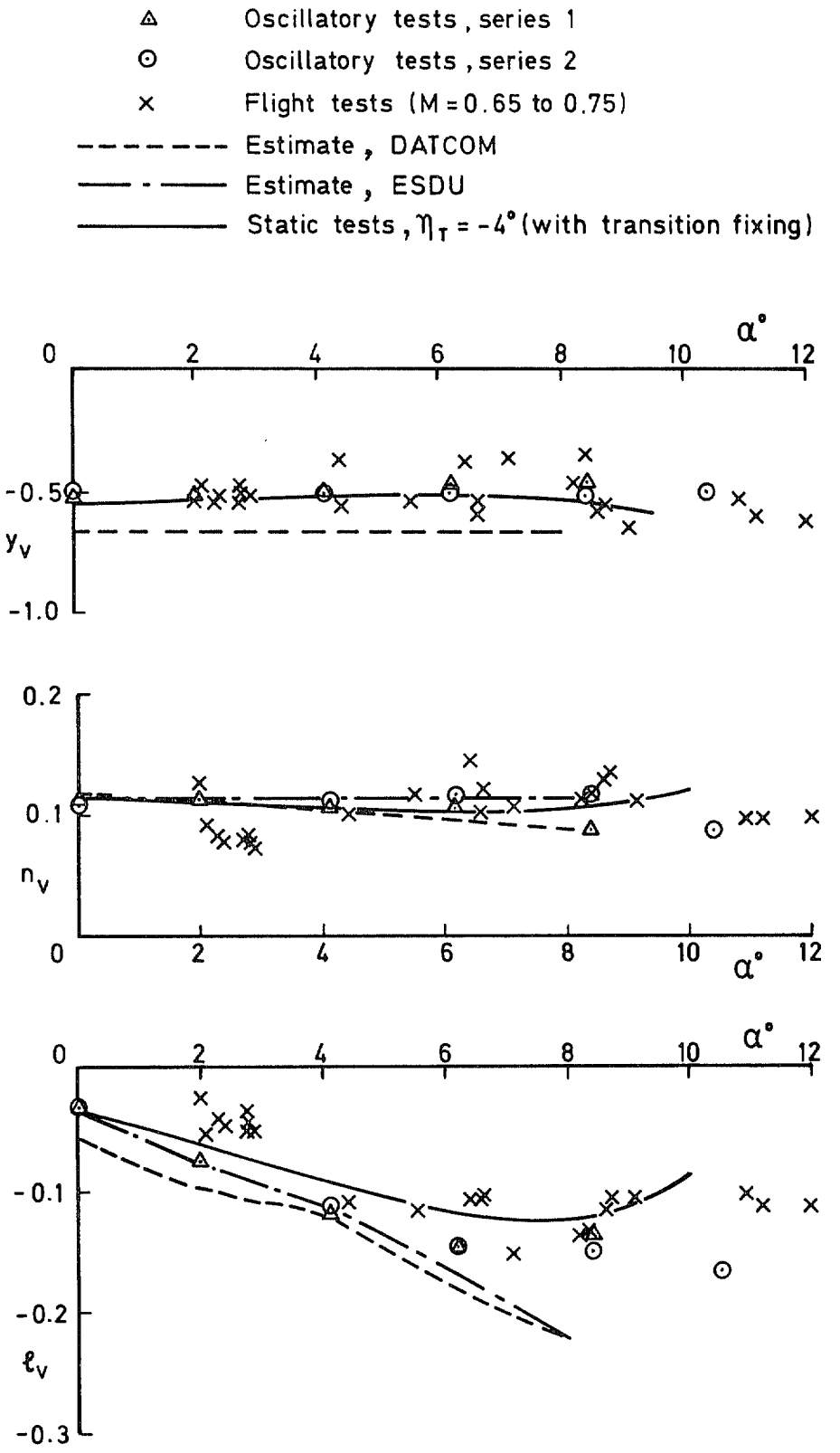

Fig 8a Derivatives due to sideslip. Fin on, M = 0.7

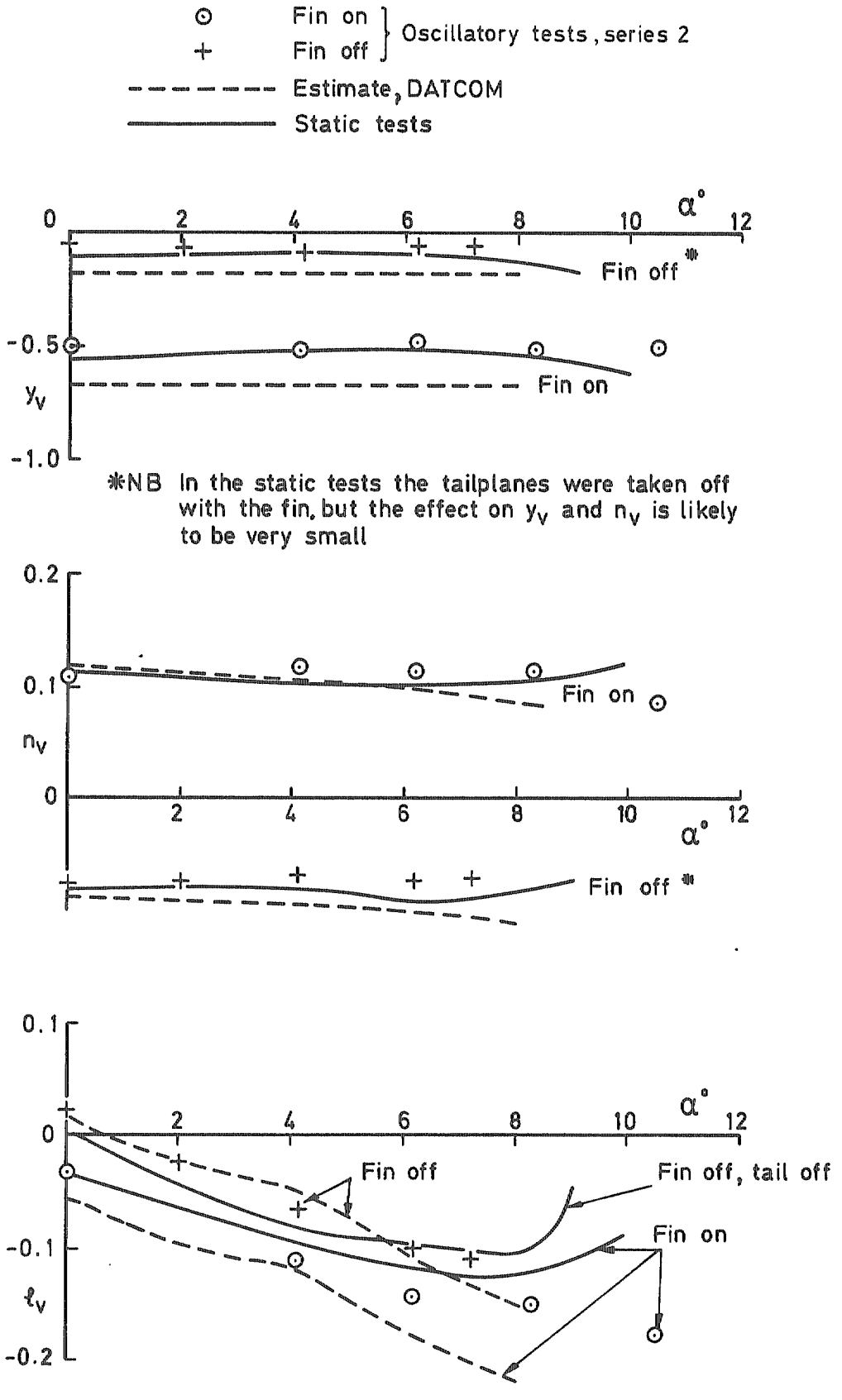

Fig 8b Derivatives due to sideslip. Fin effect, M = 0.7

Fig 9a

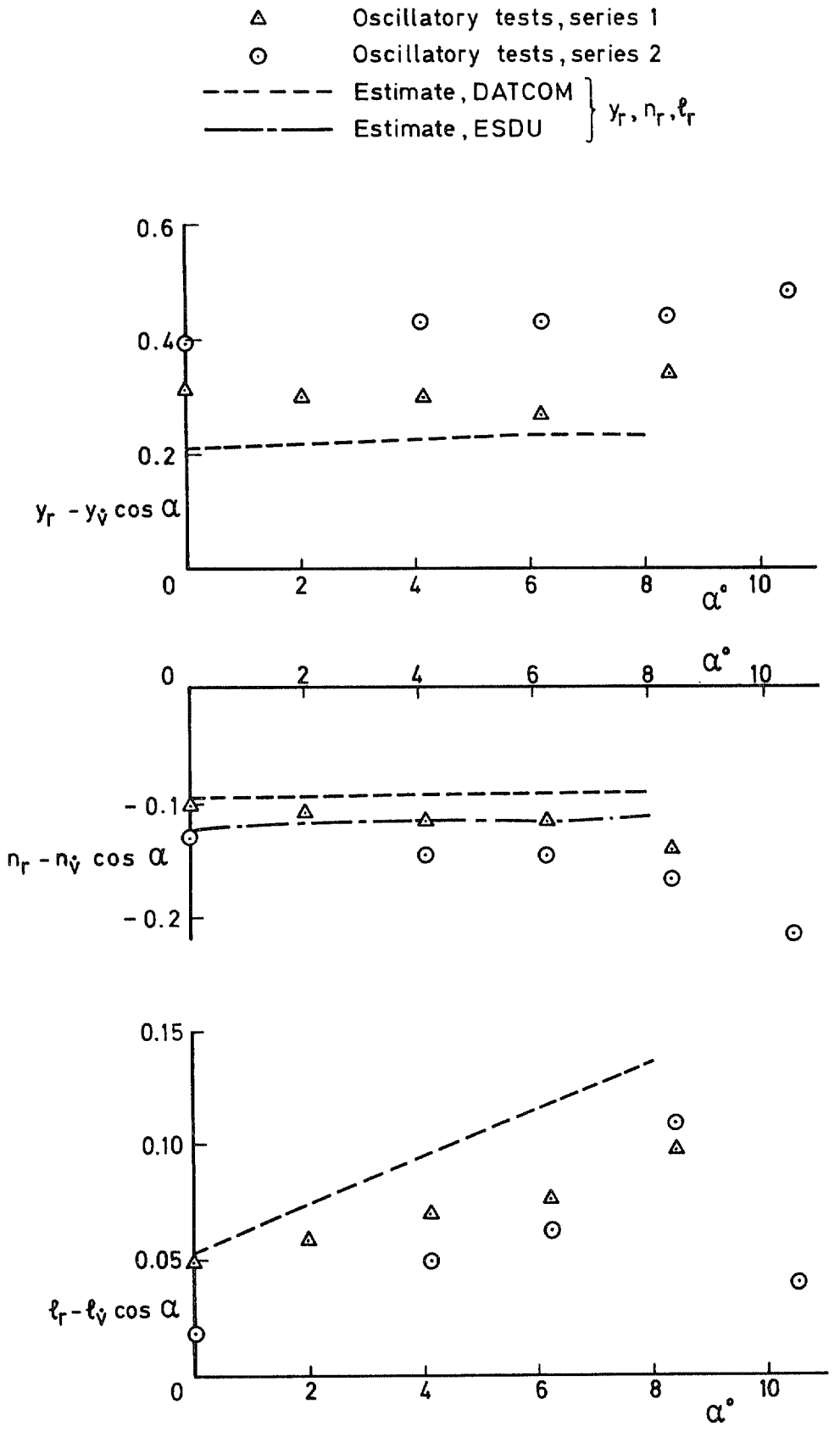

Fig 9a Derivatives due to rate of yaw. Fin on, M = 0.7

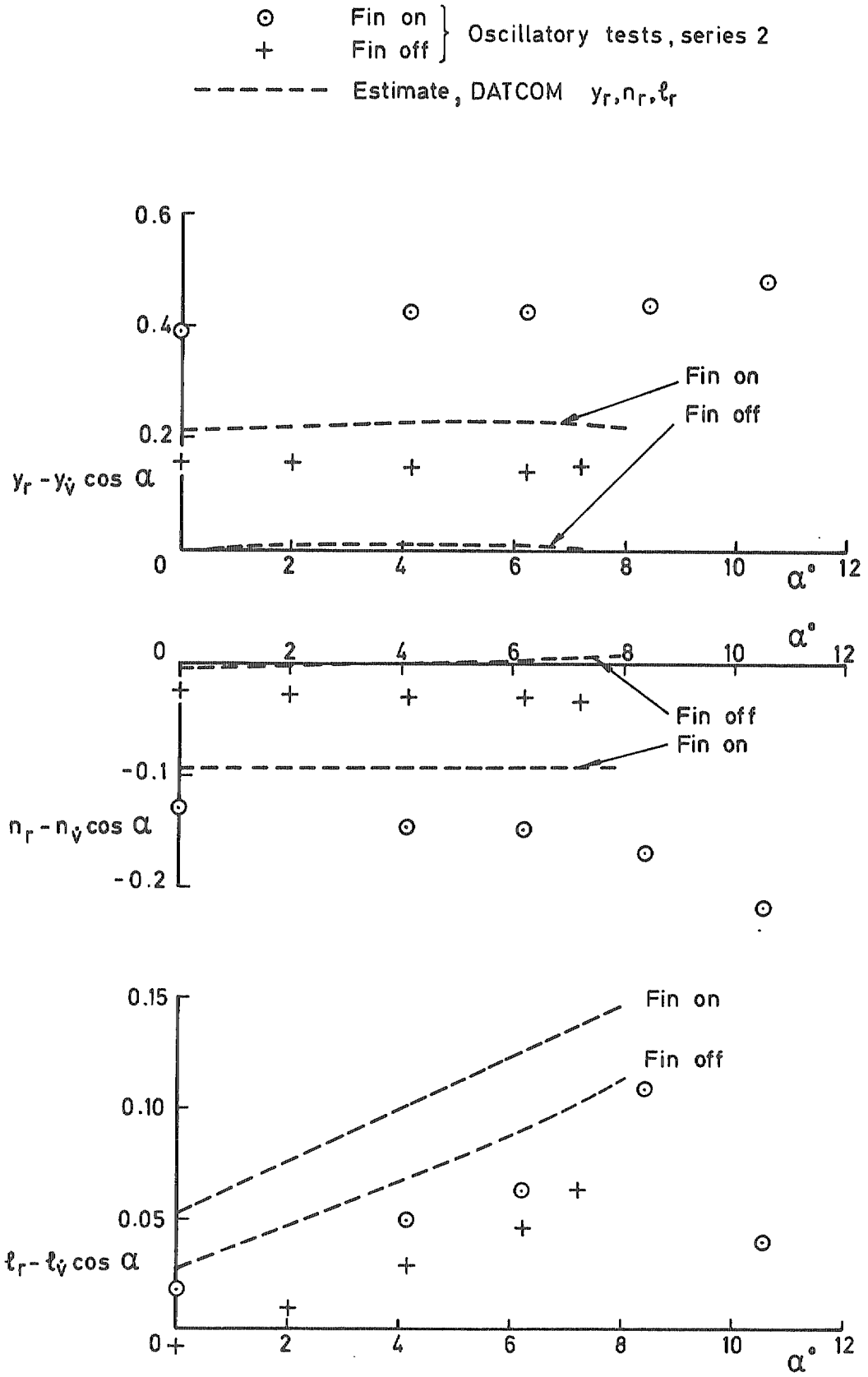

Fig 9b Derivatives due to rate of yaw. Fin effect, M = 0.7

Fig 10a

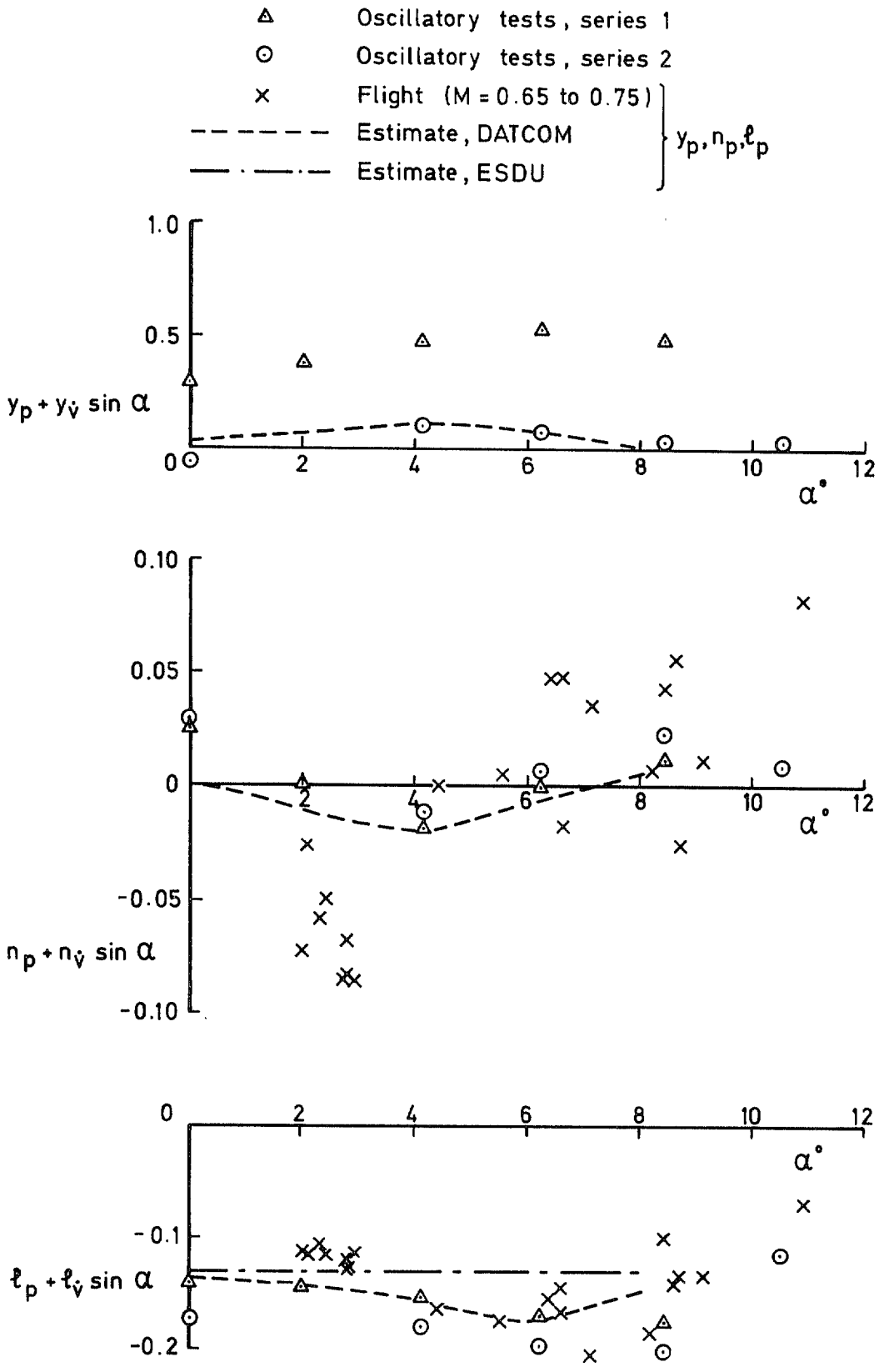

Fig 10a Derivatives due to rate of roll. Fin on, M = 0.7

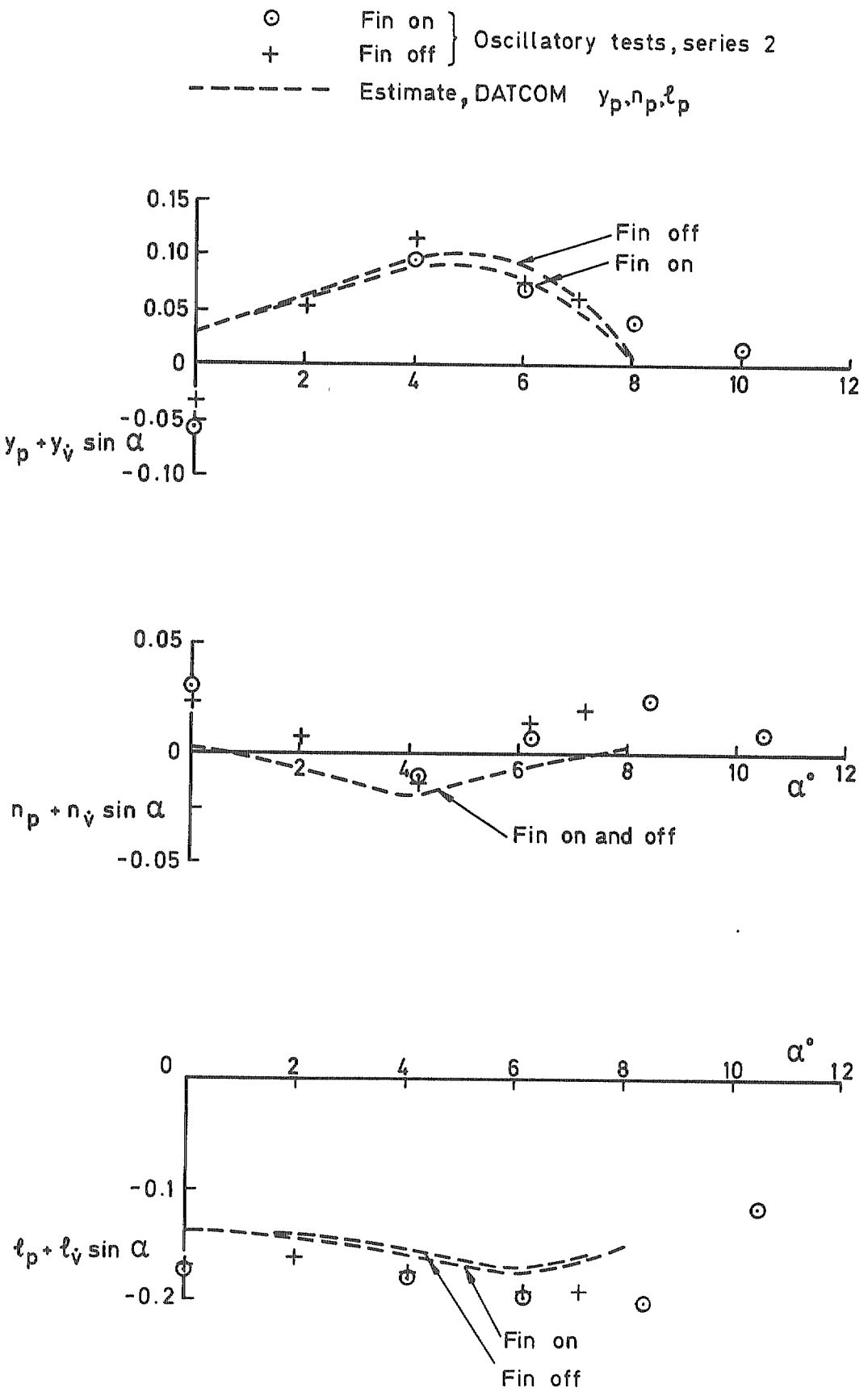

Fig 10b Derivatives due to rate of roll. Fin effect, M = 0.7

Fig 11

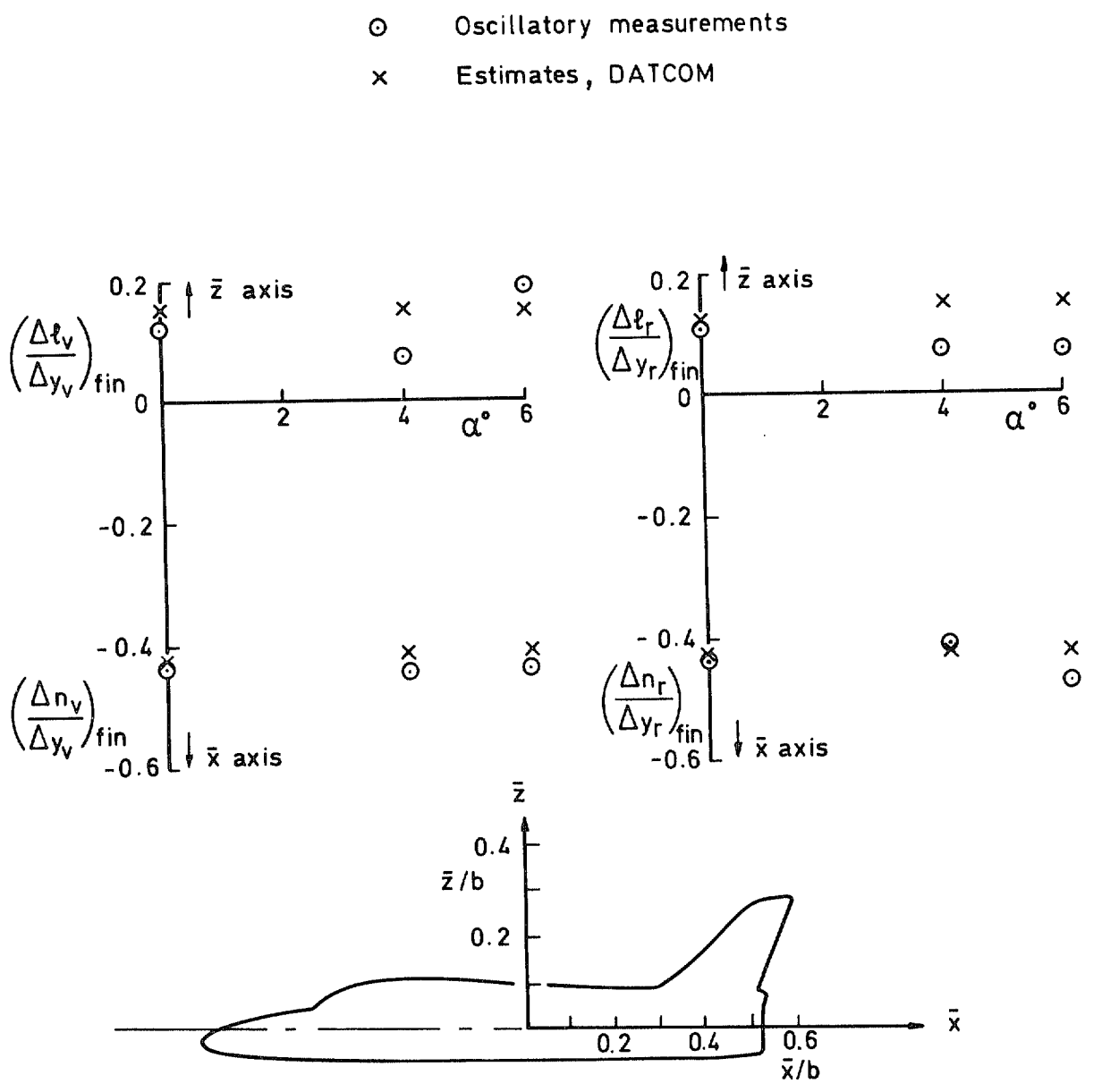

Fig 11 Effective fin-arms obtained from experiment and estimates

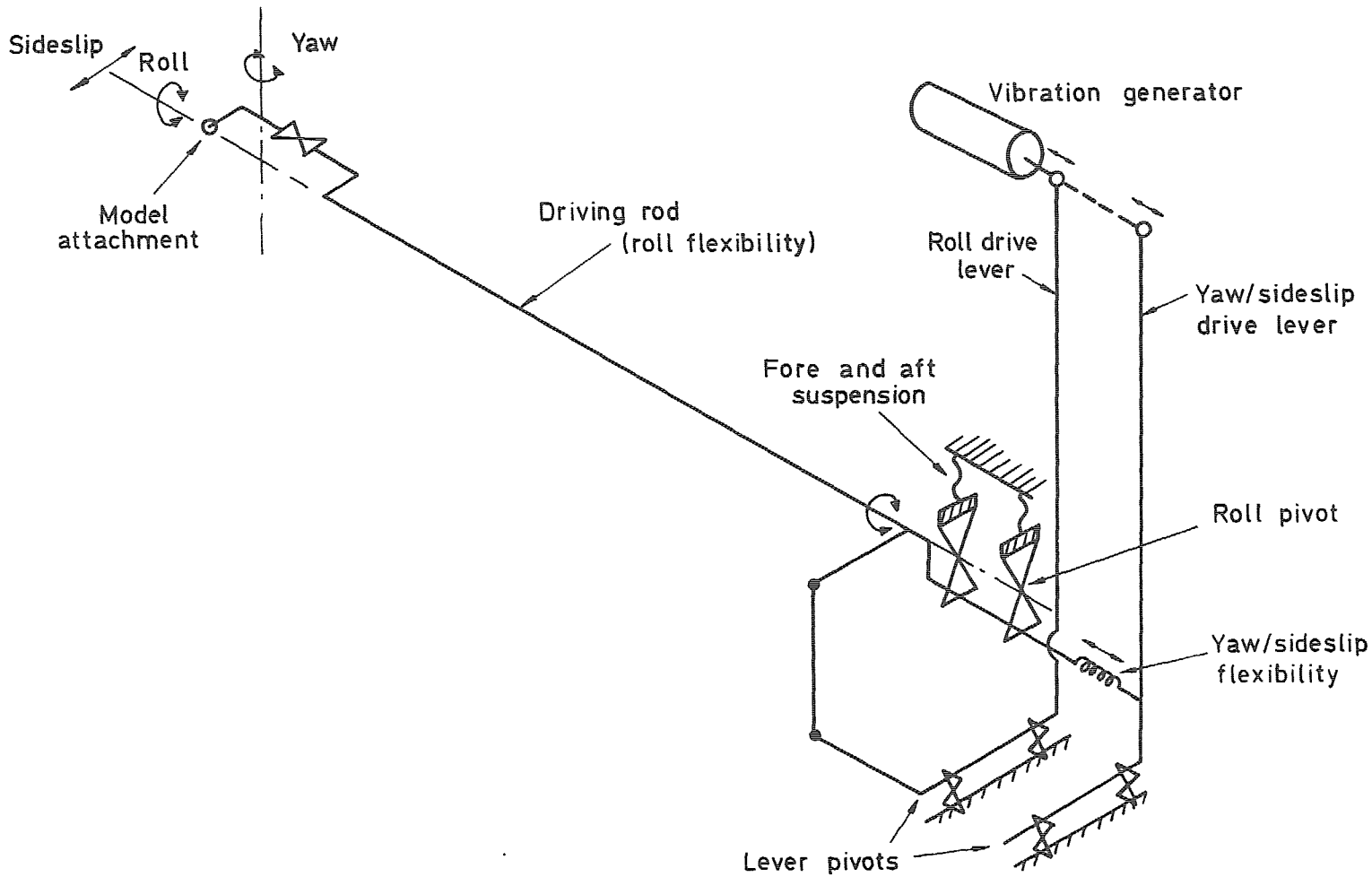

Fig 12 Proposed new drive system incorporating separate roll and yaw/sideslip drives

Printed in England for Her Majesty's Stationery Office by the Royal Aircraft Establishment, Farnborough. Dd. 596060 K4 4/80.

First published 1980

HER MAJESTY'S STATIONERY OFFICE

Government Bookshops
49 High Holborn, London WC1V 6HB
13a Castle Street, Edinburgh EH2 3AR
41 The Hayes, Cardiff CF1 1JW
Brazennose Street, Manchester M60 8AS
Southey House, Wine Street, Bristol BS1 2BQ
258 Broad Street, Birmingham B1 2HE
80 Chichester Street, Belfast BT1 4JY

Government Publications are also available through booksellers

R & M No. 3847
ISBN 011471181